Numerical Investigation of Aerosolization in the Venturi Dustiness Tester: Aerodynamics of a Particle on a Hill

Supplemental Material

Nithin Kumar Palakurthi Urmila Ghia
Mechanical and Materials Engineering
College of Engineering and Applied Science
University of Cincinnati
Cincinnati, Ohio 45221-0072

Leonid A. Turkevich
Engineering and Physical Hazards Branch (EPHB)
Division of Field Studies and Engineering (DFSE)
National Institute for Occupational Safety and Health (NIOSH)
Centers for Disease Control and Prevention (CDC)
1090 Tusculum Avenue
Cincinnati, Ohio 45226

Journal of Fluids Engineering
31 August 2021

S1 2D Flow over a Cylinder on a Flat Substrate

There are two approaches to overcome the singular contact of a cylinder on a flat plate: a) placing the cylinder above the flat plate at different heights; b) embedding the cylinder [37] at different depths into the flat plate; this latter geometry introduces additional singularities at the contact of the embedded curved particle and the flat surface, and these need to be treated with a smoothing protocol. In each approach, the lift, drag and torque, experienced by the particle, are calculated as a function of height/depth and then extrapolated to the limiting case of the particle just touching the wall.

Palakurthi *et al* [10] discussed the problem of a cylinder (2d) or a sphere (3d) in contact with a flat plate. Simulations were performed in a channel for 2 geometries: i) the particle slightly elevated over the flat plate; ii) the particle slightly embedded into the flat plate. While drag and torque were relatively insensitive to these geometries, the low Re lift was found to vary slowly with elevation height for the first geometry but to vary drastically as the embedding depth in the second geometry was reduced. Simulations were performed [10] over the particle Reynolds number range $0.01 < Re_{cyl} < 13$. We note other theoretical work on cylinders near/at walls [80-83].

Figure S1 shows the drag coefficient, $C_{drag} = F_{drag}/1/2\ \rho\ u^2$, where u is the asymptotic upstream velocity at the cylinder center (i.e. at height H). C_{drag} and the moment coefficient, C_m (not shown here), are quite insensitive to H; our calculations for C_{drag} and C_m are slightly less than those of Sweeney & Finlay [36].

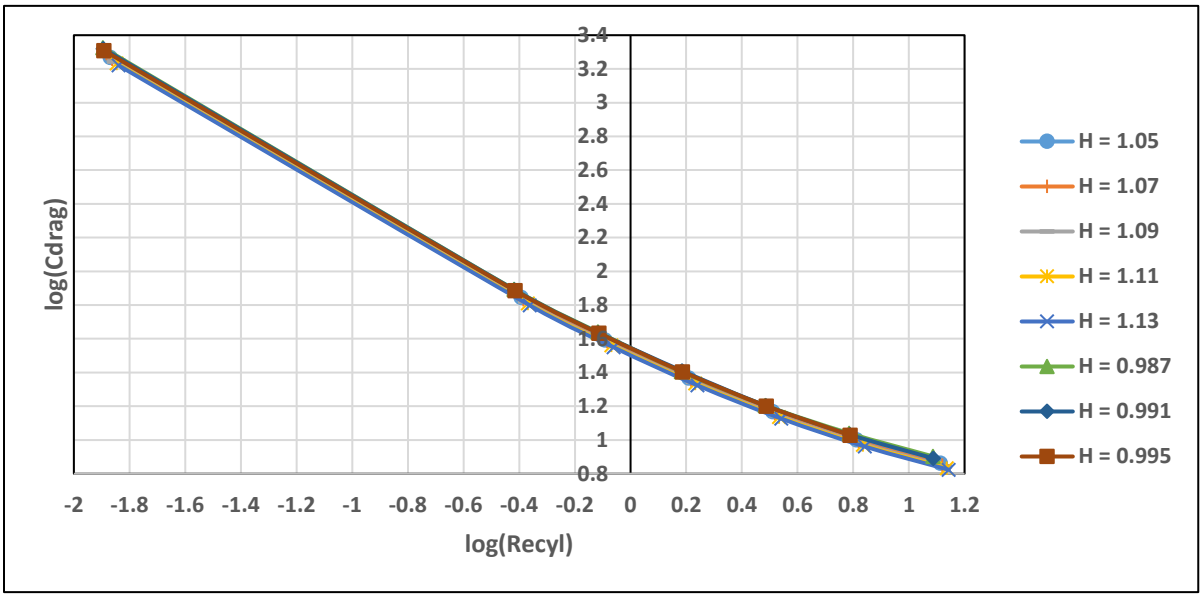

Figure S1 *Drag coefficients, for specified H/D, as a function of Cylinder Reynolds number*

Figure S2 shows the lift coefficient, $C_{lift} = F_{lift}/1/2\ \rho\ u^2$ (note the linear, not logarithmic, scale for C_{lift}). For $Re_{cyl} > 0.3$, C_{lift} is independent of H; for $Re_{cyl} < 0.3$, C_{lift} is constant and independent of H for the cylinder elevated above the plate; however, for the embedded cylinder, C_{lift} decreases dramatically as Re_{cyl} is reduced, even going negative with greater decrease for the greater embedding distance (smaller H). Our values for C_{lift} are always less than those of Sweeney &

Finlay [36], who use the embedded geometry; the Sweeney-Finlay lift is always positive due to the upward vertical velocity in the Blasius layer (vertical velocity = 0 in our axial shear problem). This upward vertical velocity will again become important for the problem of the test particle on a hill. Palakurthi *et al* (2017) discuss the origin of the negative lift for the embedded cylinder.

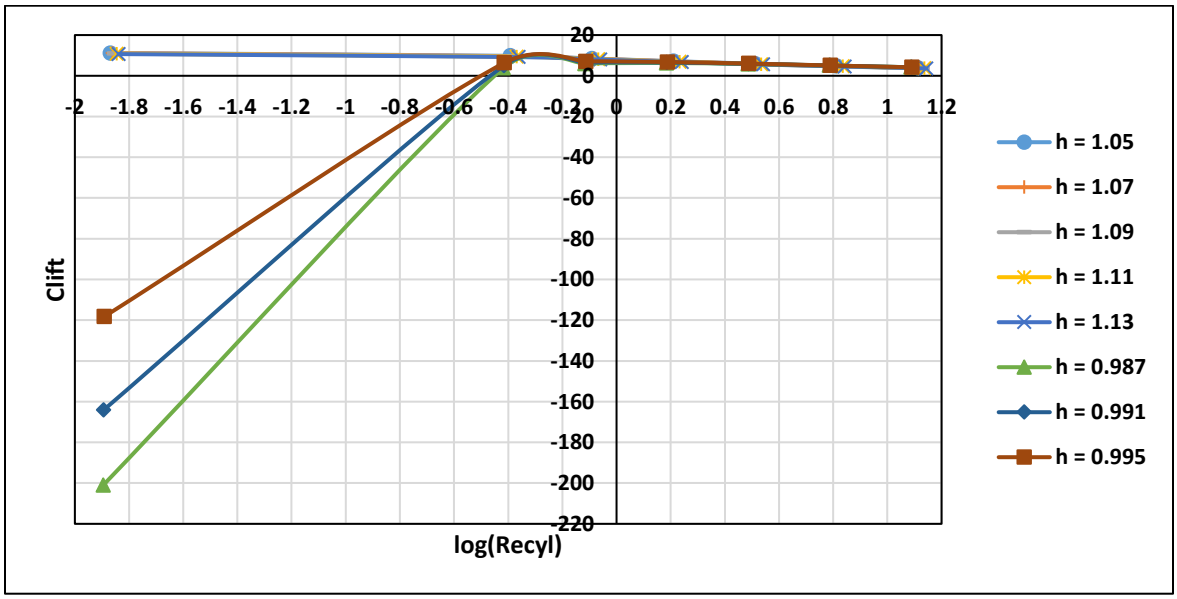

Figure S2 *Lift coefficients, for specified H/D, as a function of Cylinder Reynolds number*

Palakurthi *et al* [10] also discuss the grid convergence of these results.

802

S2 3D Flow over a Sphere on a Flat Substrate

804 In 3d, a similar approach is carried out [10] for a sphere in the vicinity of a flat substrate for 0.01
805 < Re_{sph} < 24. For the sphere above the flat plate, H = 1.05; for the embedded sphere, H = 0.995.
806 We note other theoretical work near/at walls [84-94].

807

808 **Figures S3** and **S4** present coefficients of drag and lift plotted with respect to Re_{sph}

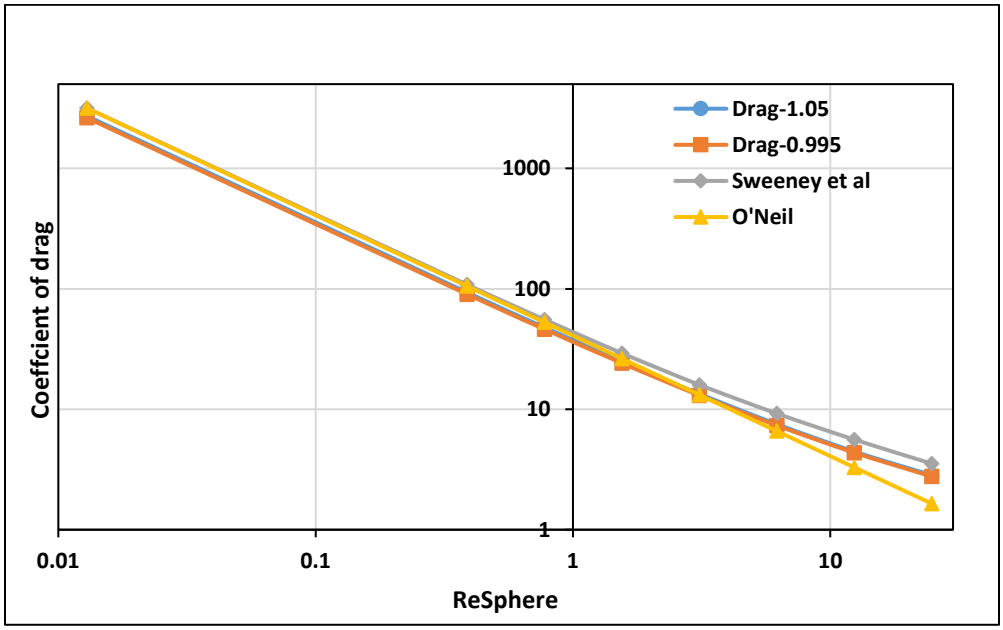

809

810 ***Figure S3*** *Drag coefficient for the sphere above and embedded into the flat plate.*

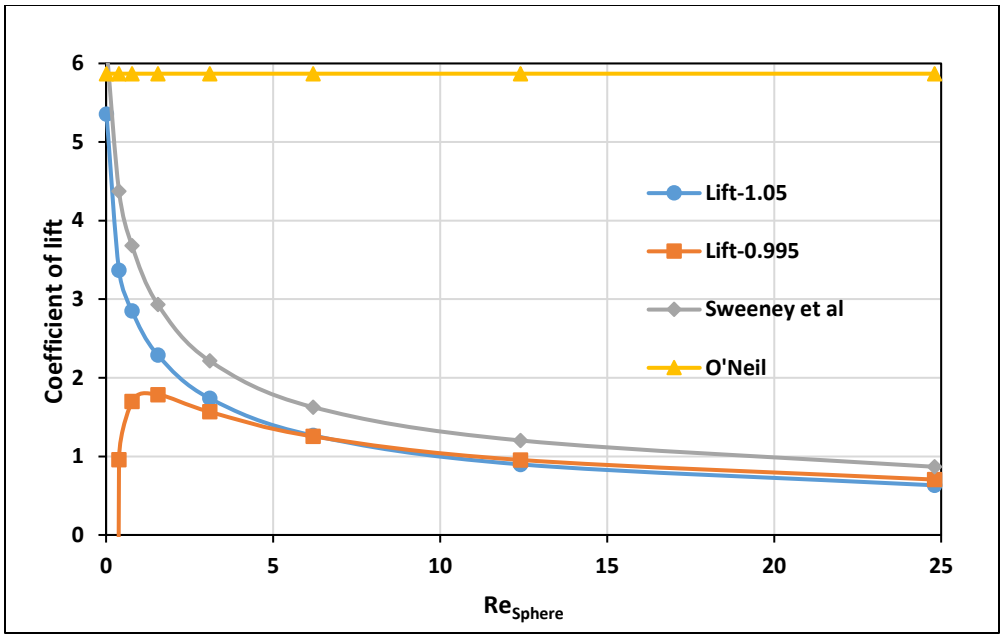

Figure S4 *Lift coefficient for the sphere above and embedded into the flat plate*

C_{drag} is relatively independent of H and agrees with Sweeney & Finlay [36] and with the analytical (Stokes flow) results of O'Neill [25], even though the latter is only valid for low Re_{sph}. For H = 1.05, C_{lift} agrees with Sweeney & Finlay [36], and, at lower Re_{sph}, C_{lift} approaches the result of Leighton & Acrivos [26]. For H = 0.995, $C_{lift} < 0$ for the lowest Re_{sph}, similar to the 2d case of the embedded cylinder.

Palakurthi *et al* [10] discuss the grid convergence of these results.

S3 Parametric Study

We discuss the effect of varying the wedge height, L, and the cylinder diameter, D.

S.3.1 Wedge height

We have studied the dependence of the drag and lift forces on the wedge height, L. Using a fixed cylinder size (D = 2 mm), fixed cylinder location near the wedge summit (θ = 80°), and fixed wedge half-angle α = 60°, three wedge heights were considered: L = 7 mm, L = 13 mm and L = 19 mm. The normalized drag increases with wedge height; it also exhibits a minimum at intermediate Re, which becomes more apparent at the higher wedge heights (**Figure S5**).

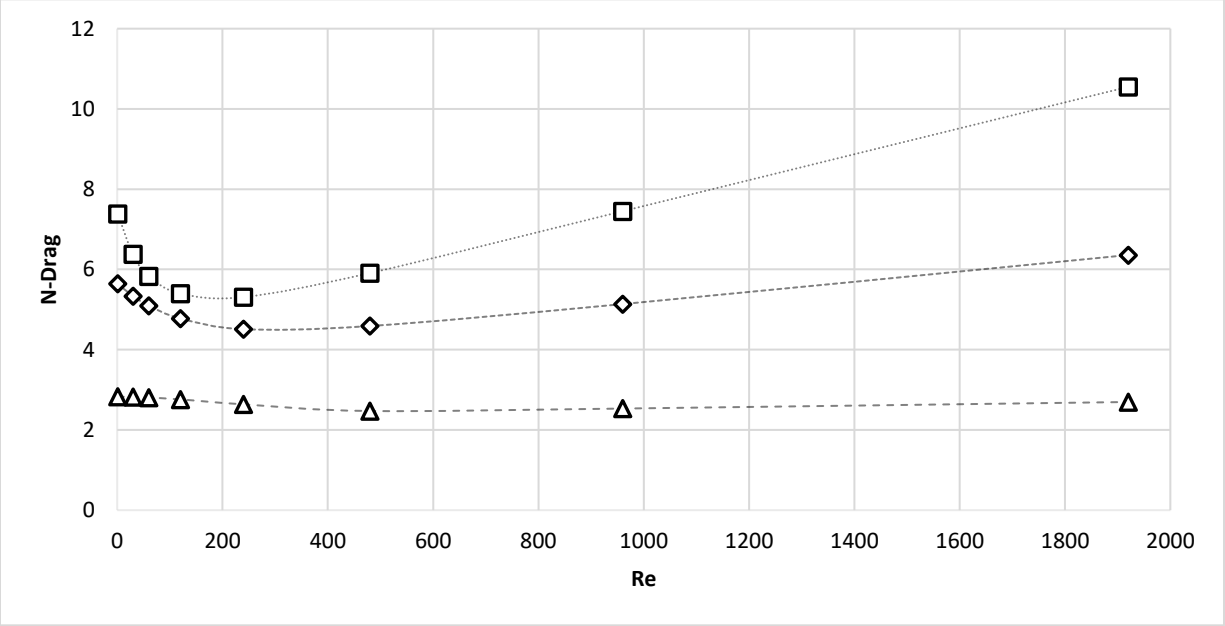

Figure S5. *Normalized drag $F_{drag}(\theta)/F_{drag}(0)$ for the cylinder on 3 different wedge heights (α = 45°, θ = 80°): L = 7 mm (triangle), L = 13 mm (diamond), L = 19 mm (square).*

The normalized lift increases with wedge height and monotonically increases with Reynolds number (**Figure S6**).

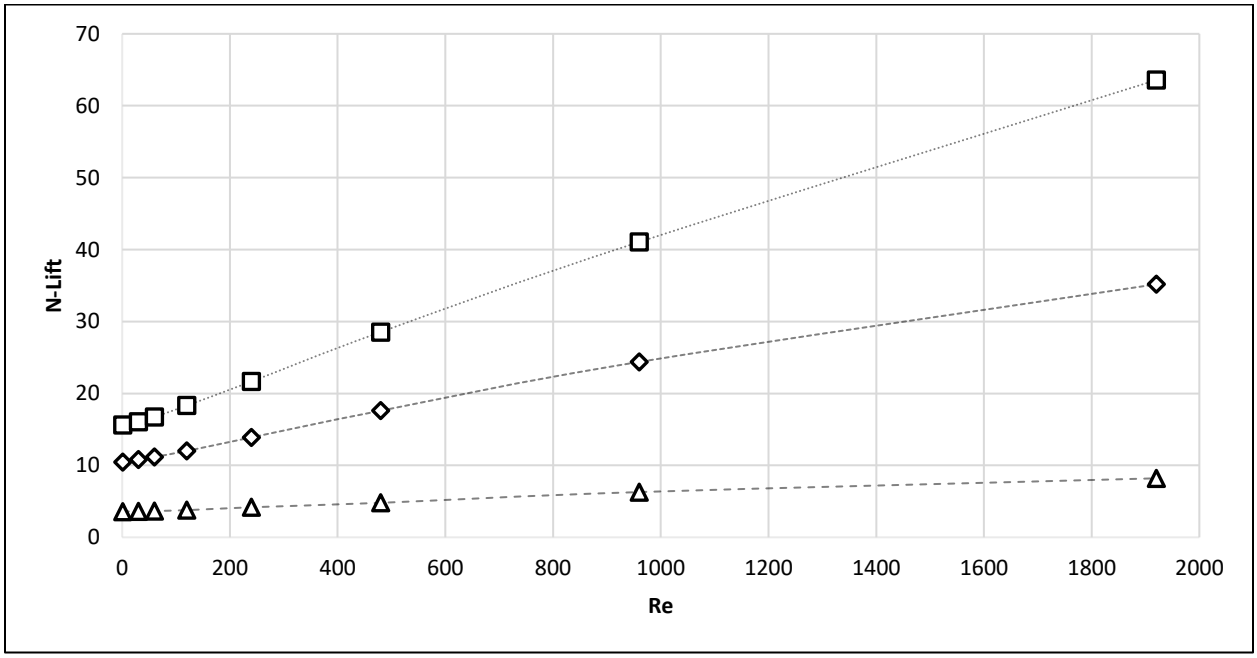

Figure S6. *Normalized lift, $F_{lift}(\theta)/F_{lift}(0$ for the cylinder on 3 different wedge heights (α = 45°, θ = 80°): L = 7 mm (triangle), L = 13 mm (diamond), L = 19 mm (square).*

S.3.2 Cylinder Diameter

We have studied the dependence of the drag, moment and lift on the cylinder diameter D. Using a fixed wedge height H = 13 mm, fixed wedge half-angle α = 60°, and fixed cylinder location on the wedge (θ = 60°), three cylinder diameters were considered: D = 0.5 mm, D = 1 mm and D = 2 mm.

As the diameter of the cylinder decreases, the normalized drag (**Figure S7**) does not vary appreciably

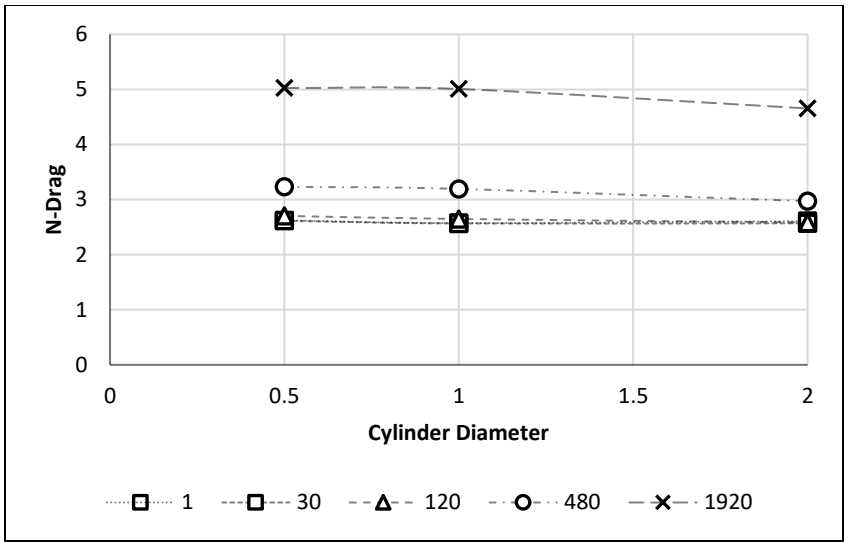

Figure S7. *Normalized drag $F_{drag}(\theta)/F_{drag}(0)$ for the different cylinder diameters on a wedge α = 60°, θ = 60°, height L = 13mm.*

As the diameter of the cylinder decreases, the normalized lift increases (**Figure S8**).

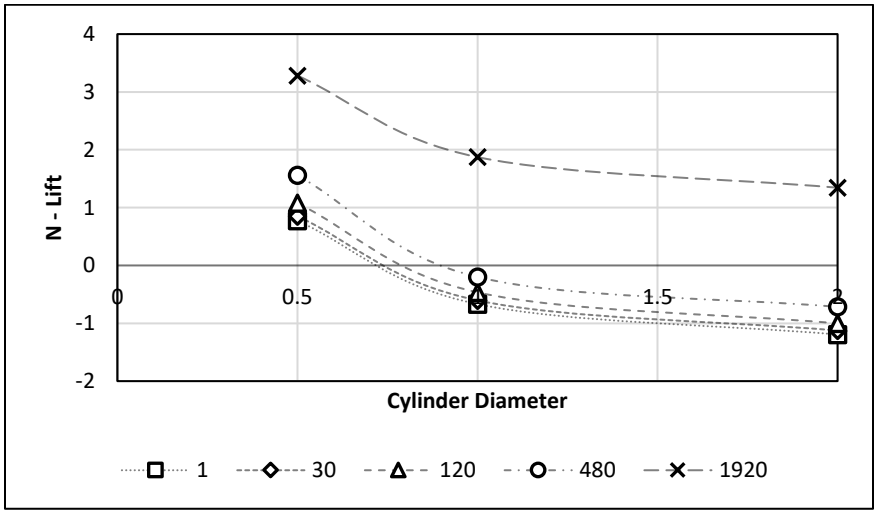

Figure S8. *Normalized lift, $F_{lift}(\theta)/F_{lift}(0$ for the different cylinder diameters on a wedge α = 60°, θ = 60°, height L = 13mm*

S4 Origin of the Enhanced Drag and Lift—2D Cylinder on the Wedge

In this section we analyze the origin of the enhanced drag and lift on the cylinder as it is located up and then down the wedge. We consider the special case of Re = 1 and wedge angle $\alpha = 45^{o}$ (streamlines displayed in **Figure S9**).

a)

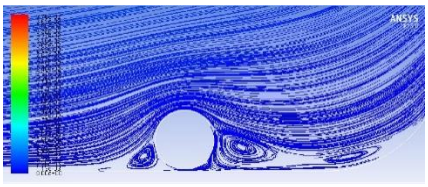

b)

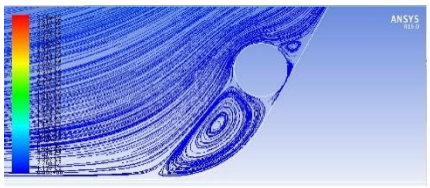

c)

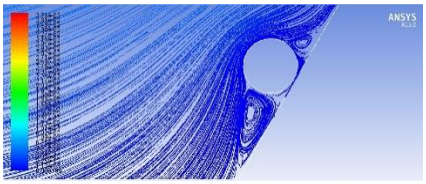

d)

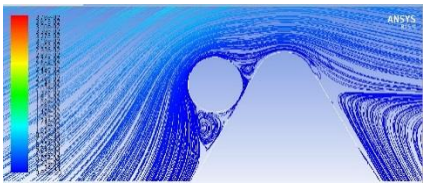

e)

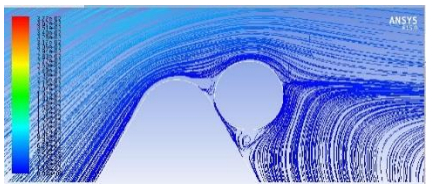

f)

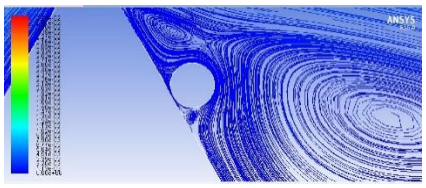

g)

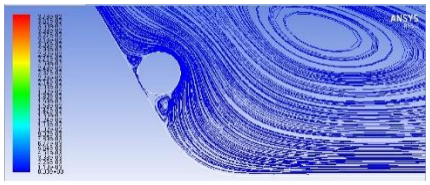

h)

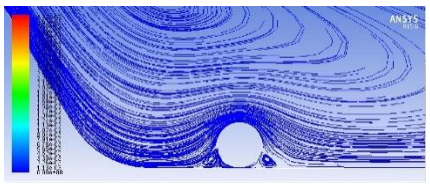

Figure S9 *Streamlines for the flow around the cylinder positioned at different locations, θ, on the wedge: a) θ = 0°, b) θ = 30°, c) θ = 60°, d) θ = 80°, e) θ = 100°, f) θ = 120°, g) θ = 150°, h) θ = 180°. Flow is left-to-right.*

It is useful to consider the pressure, p, and shear stress, τ, around the surface of the test cylinder. Let χ be the polar angle around the cylinder, with standard orientation, i.e. $\chi = 0$ is the horizontal (downstream of the flow), $\chi = \pi/2$ is the vertical (top of the cylinder) exposed to the flow, $\chi = \pm \pi$ is the horizontal (upstream of the flow), $\chi = -\pi/2$ is the sheltered vertical (bottom of the cylinder) closest to the substrate. We look at p and τ for various locations, θ, of the cylinder on the wedge: $\theta = 0^o$ (upstream of the wedge), $\theta = 80^o$ (upstream approaching the apex), $\theta = 100^o$ (downstream past the apex), $\theta = 180^o$ (downstream of the wedge).

Figure S10 displays the evolution of $p(\chi)$ as the cylinder is moved up the wedge ($0^o < \theta < 80^o$). Upstream of the wedge ($\theta = 0^o$), the pressure is depressed behind the cylinder ($\chi = 0$) and enhanced at the stagnation point ahead of the cylinder ($\chi = \pm \pi$); both downstream depression and upstream enhancement are amplified as the cylinder is moved up the wedge ($\theta = 80^o$).

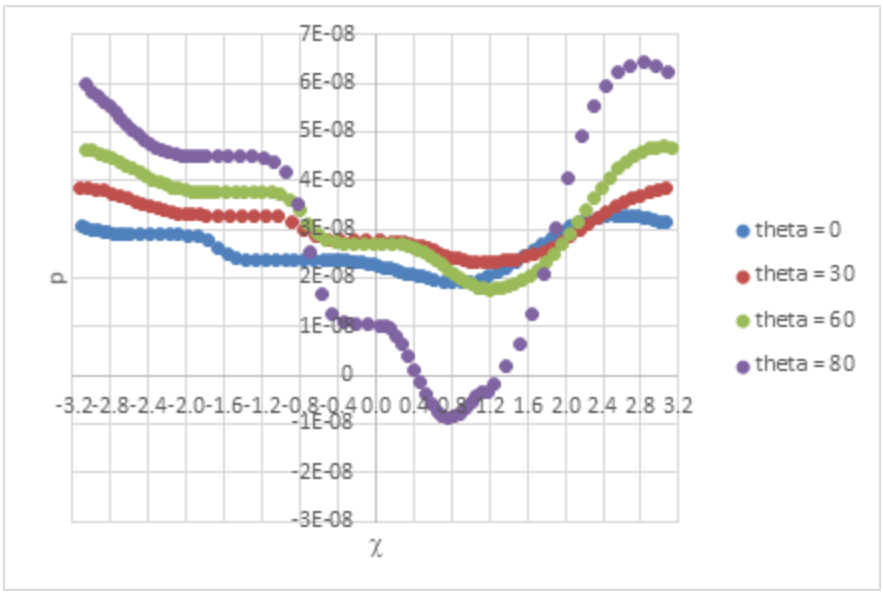

887

888 ***Figure S10*** *Pressure p(χ) around the cylinder, located on the uphill side of the wedge; Re = 1.*

889 **Figures S11** and **S12** trace the effect of this change in p(χ) on the pressure contribution to the drag

890 and lift.

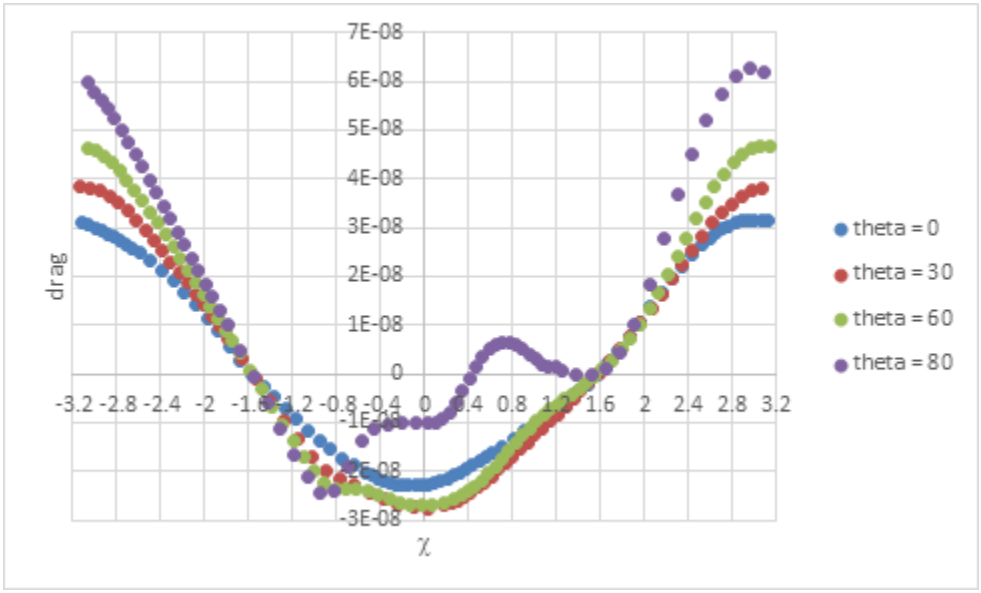

891

892 ***Figure S11*** *Contribution of the pressure to the drag for the cylinder located on the uphill side*

893 *of the wedge; Re = 1.*

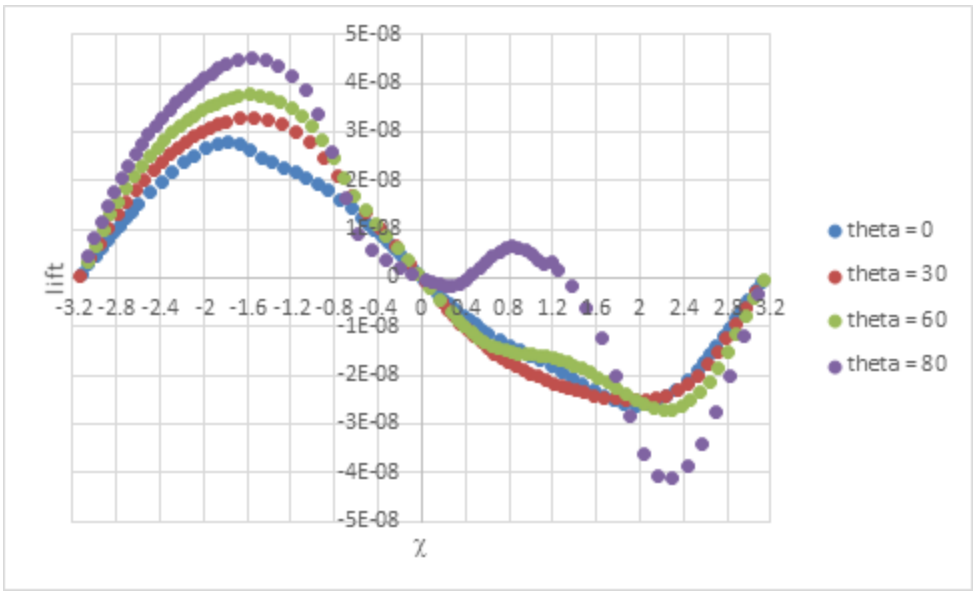

894

895 ***Figure S12*** *Contribution of the pressure to the lift for the cylinder located on the uphill side of*

896 *the wedge; Re = 1.*

897

898 The cancellation between positive (upstream) and negative (downstream) contributions to the drag

899 gives rise to the small drag of the cylinder on the flat plate; this cancellation is less effective as the

900 cylinder is moved up the wedge. The cancellation between positive (bottom) and negative (top)

901 contributions to the lift gives rise to the small lift of the cylinder on the flat plate; this cancellation

902 is also less effective as the cylinder is moved up the wedge.

903 In **Figure S13**, as the cylinder is moved down the wedge, downstream of the apex ($100^o < \theta <$

904 180^o), the amplified pressure variation is undone.

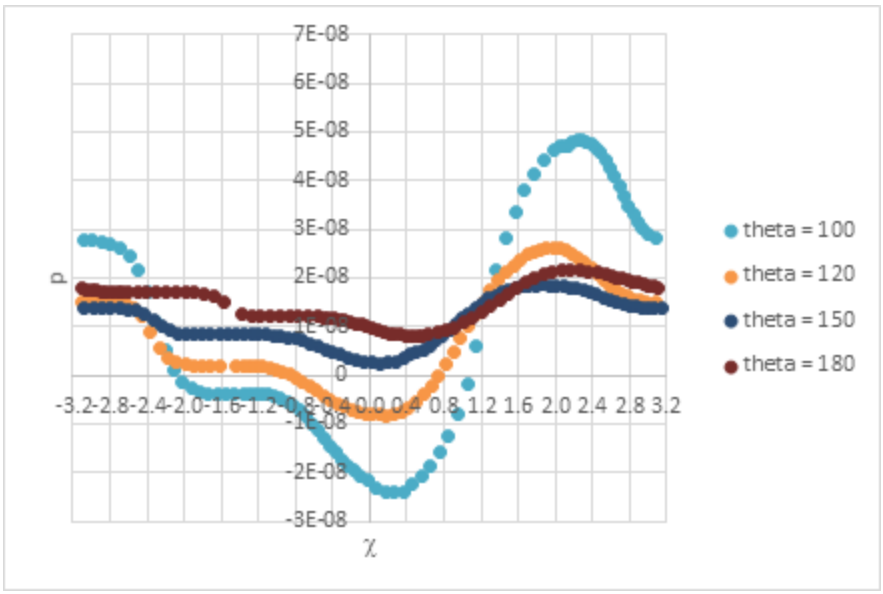

905

906 ***Figure S13*** *Pressure p(χ) around the cylinder, located on the downhill side of the wedge; Re =*

907 *1.*

908

909 **Figures S14** and **S15** trace the effect of this change in p(χ) on the pressure contribution to the drag

910 and lift.

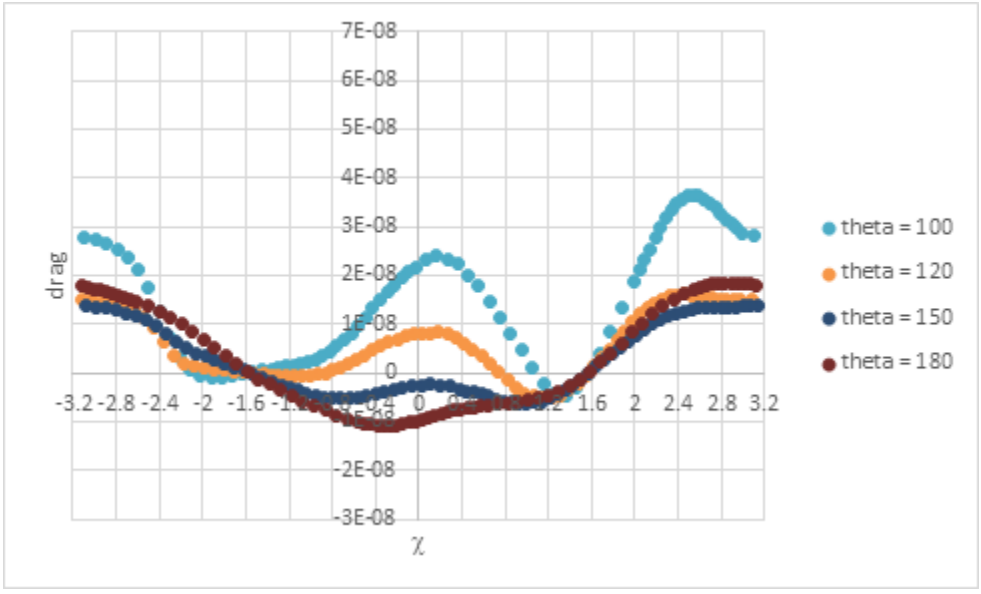

911

Figure S14 *Contribution of the pressure to the drag for the cylinder located on the downhill side of the wedge; Re = 1.*

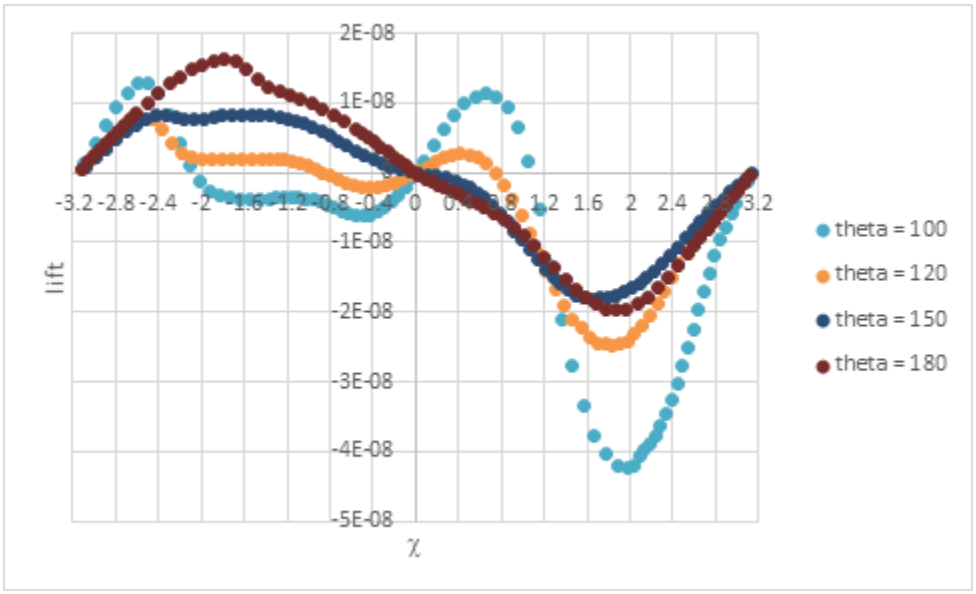

Figure S15 *Contribution of the pressure to the lift for the cylinder located on the downhill side of the wedge; Re = 1.*

Figure S16 displays the evolution of $\tau(\chi)$ as the cylinder is moved up the wedge ($0^o < \theta < 80^o$). Upstream of the wedge ($\theta = 0$), all the shear stress occurs near the exposed top of the cylinder ($\chi = \pi/2$); there is no contribution to the shear stress from the side of the cylinder closest to the substrate ($\chi = -\pi/2$). As the cylinder is moved up the wedge ($0^o < \theta < 80^o$); the shear stress is amplified and is also shifted slightly downstream (i.e. over the top of the cylinder).

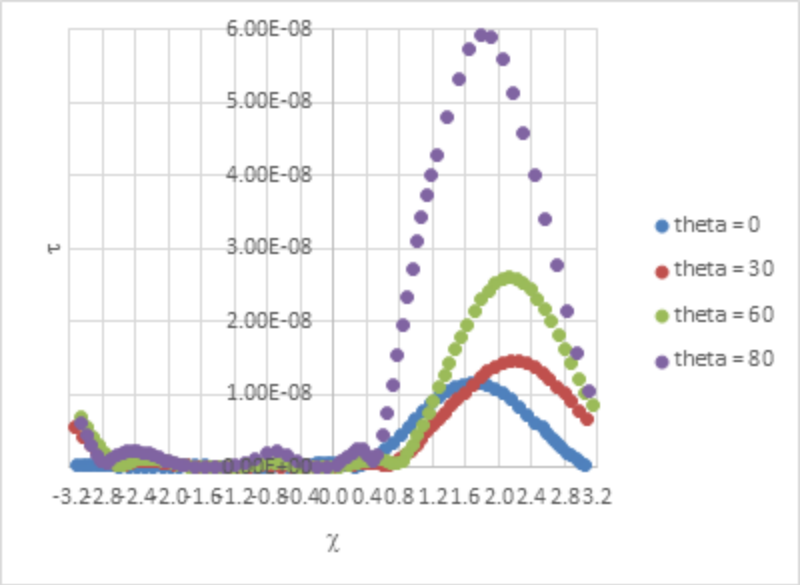

924

925

926 ***Figure S16*** *Shear stress τ(χ) around the cylinder, located on the uphill side of the wedge; Re*

927 *= 1.*

928

929 **Figures S17** and **S18** trace the effect of this change in τ(χ) on the shear contribution to the drag

930 and lift.

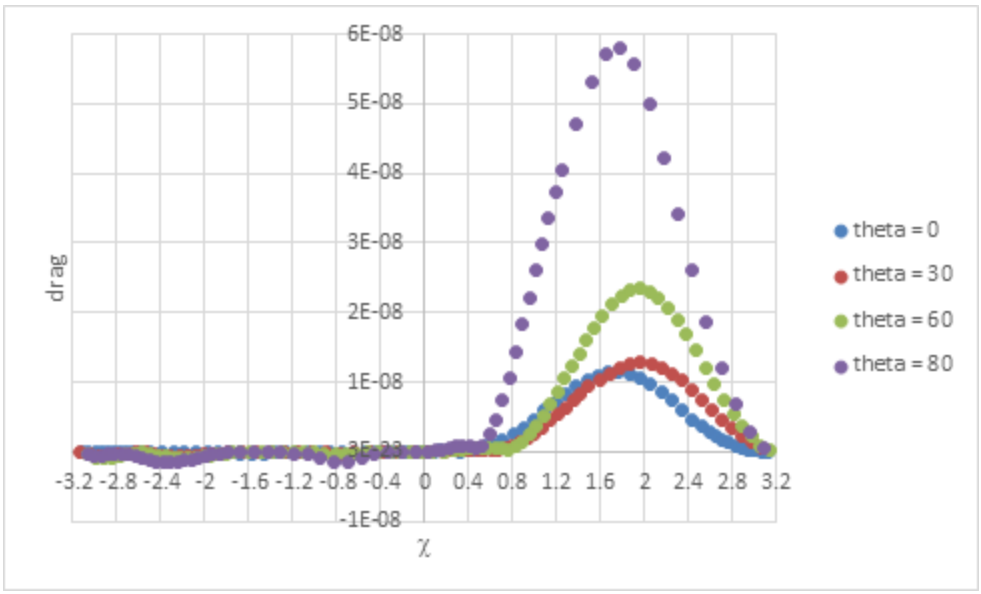

931

932 ***Figure S17*** *Contribution of the shear stress to the drag for the cylinder located on the uphill*

933 *side of the wedge; Re = 1.*

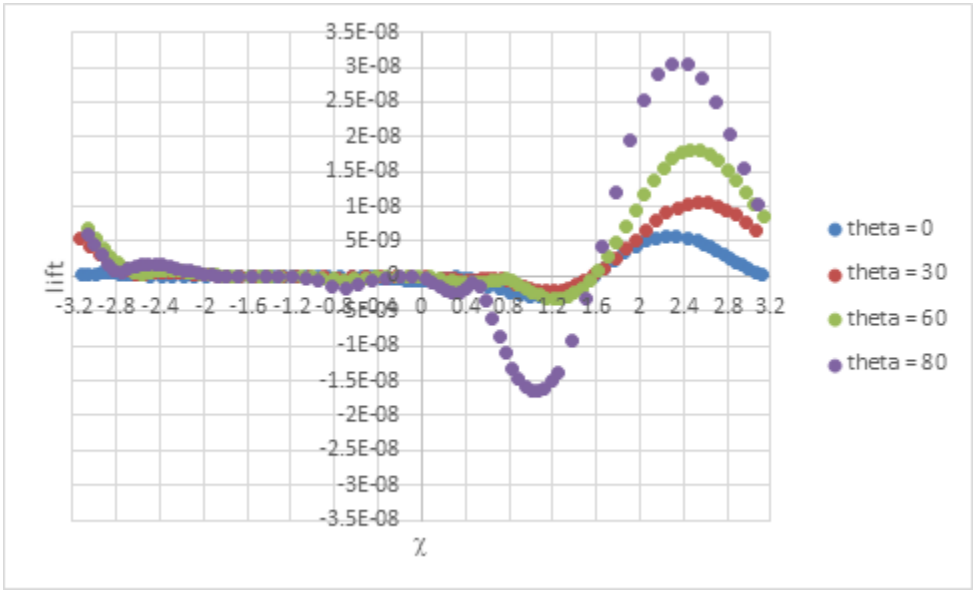

934

935 ***Figure S18*** *Contribution of the shear stress to the lift for the cylinder located on the uphill side*

936 *of the wedge; Re = 1.*

937

The shear (maximal at the top of the cylinder) always contributes positively to the drag. The shear contributes to the lift positively on the top upstream portion of the cylinder and negatively on the top downstream portion of the cylinder. The incomplete cancelation results in a small lift of the cylinder on the flat plate; as the cylinder is moved up the wedge, this cancelation becomes less effective, resulting in a higher lift due to shear.

In **Figure S19**, as the cylinder is moved down the wedge, downstream of the apex ($100^o < \theta < 180^o$), the amplified shear stress variation is undone; note also that the maximum shear stress has shifted slightly upstream (i.e.in front of the cylinder top). This slight shift (behind the cylinder top on the upstream side of the wedge, and ahead of the cylinder top on the downstream side of the wedge) in the maximum shear stress is reflected in the relative strength of positive and negative contributions to the lift.

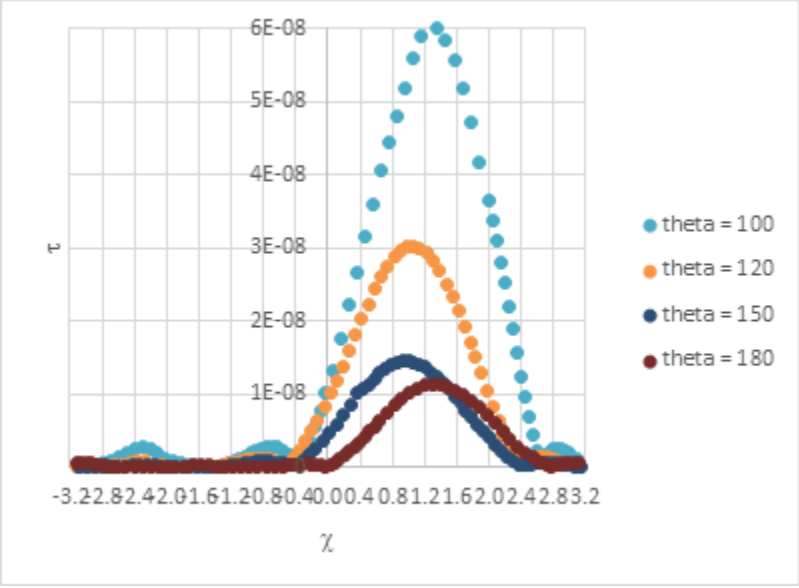

Figure S19 *Shear stress $\tau(\chi)$ around the cylinder, located on the downhill side of the wedge; Re = 1.*

Figures S20 and **S21** trace the effect of this change in $\tau(\chi)$ on the shear contribution to the drag and lift.

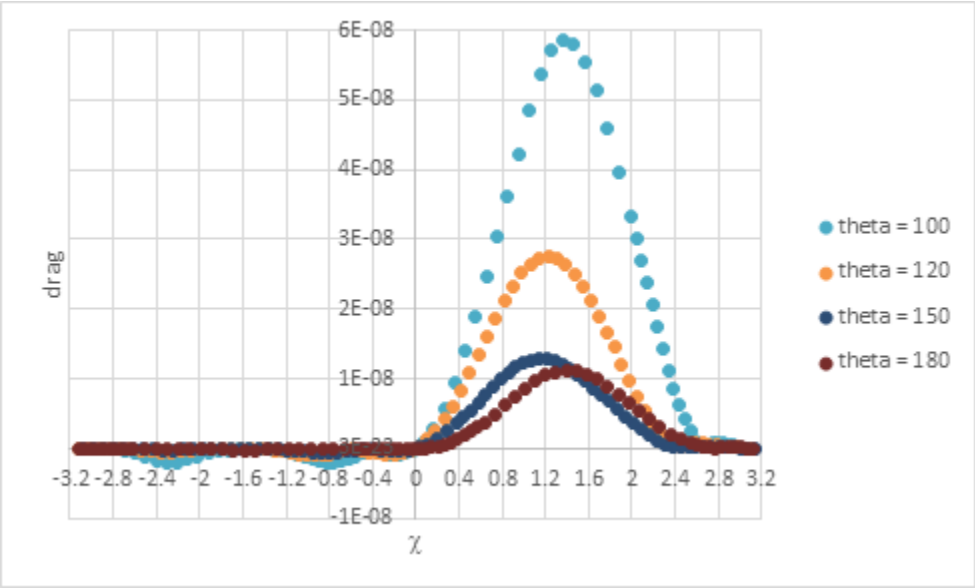

Figure S20 *Contribution of the shear stress to the drag for the cylinder located on the downhill side of the wedge; Re = 1.*

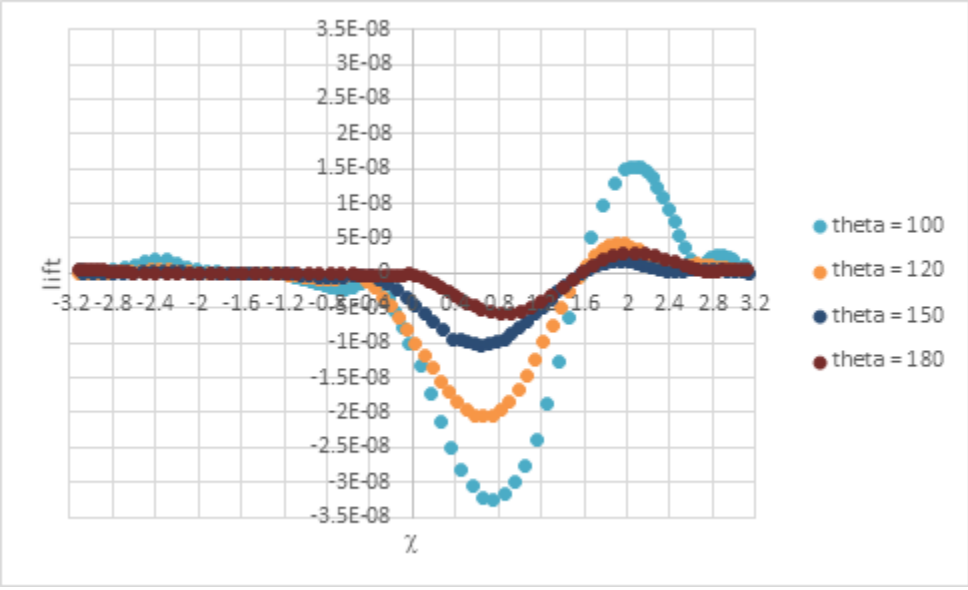

Figure S21 *Contribution of the shear stress to the lift for the cylinder located on the downhill side of the wedge; Re = 1.*

Because the maximal shear has shifted downstream of the cylinder top, the incomplete cancelation becomes negative, resulting in an overall negative shear contribution to the lift.

Integrating around the surface of the cylinder $\int d\chi$, yields the pressure and shear contributions to the drag (**Figure S22**) and lift (**Figure S23**)

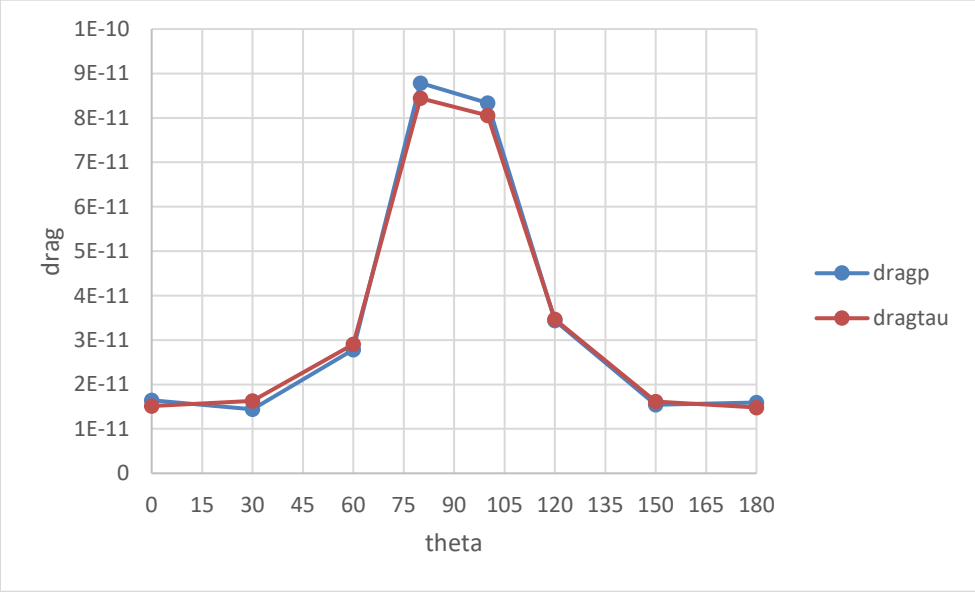

Figure S22 *Pressure and shear contributions to the drag for the cylinder at various locations, θ, on the wedge.*

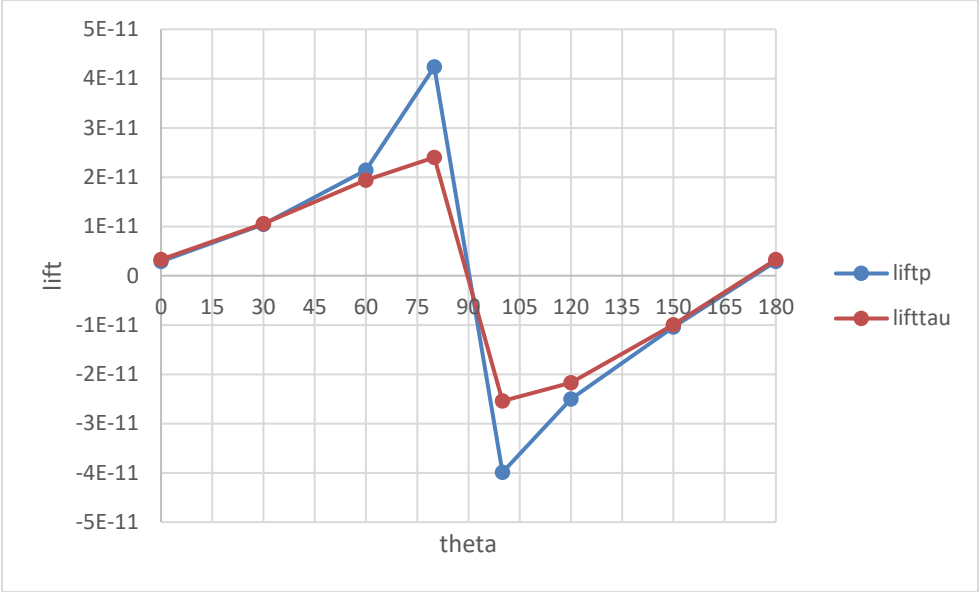

970

971 ***Figure S23*** *Pressure and shear contributions to the lift for the cylinder at various locations, θ,*

972 *on the wedge.*

973

974 Figures S22 and S23 confirm that pressure and shear contribute equally to both drag and lift, as

975 they should in the creeping flow regime (Re = 1).

976

Additional References for the Supplemental Material

[80] Dennis, S. C. R. & Chang, G. Z. (1970). Numerical solutions for steady flow past a circular cylinder at Reynolds numbers up to 100. *J. Fluid Mech.*, *42*: 471-489.

[81] Bearman, P. W. & Zdravkovich, M. M. (1978). Flow around a circular cylinder near a plane boundary. *J. Fluid Mech.*, *89*: 33-47.

[82] Vada, T., Nestegard, A., Skomedal, N. (1989). Simulation of viscous flow around a circular cylinder in the boundary layer near a wall. *J. Fluids Structures*, *3*: 579-594.

[83] Zovatto, L. & Pedrizzetti, G. (2001). Flow about a circular cylinder between parallel walls. *J. Fluid Mech.*, *440*: 1-25.

[84] Legendre, D. & Magnaudet, J. (1997). A note on the lift force on a spherical bubble or drop in a low-Reynolds-number shear flow. *Phys. Fluids*, *9*: 3572-3574.

[85] Drew, D.A. (1988). The lift force on a small sphere in the presence of a wall. *Chem. Eng. Sci. 43*: 769-773.

[86] Asmolov, E. S. (1990). Dynamics of a spherical particle in a laminar boundary layer. *Fluid Dynamics*, *25*: 886-890.

[87] Asmolov, E. S. (1999). The inertial lift on a spherical particle in a plane Poiseuille flow at large channel Reynolds number. *J. Fluid Mech.*, *381*: 63-87.

[88] Mei, R. (1992). An approximate expression for the shear lift force on a spherical particle at finite Reynolds number. *Int. J. Multiphase Flow*, *18*: 145-147.

[89] McLaughlin, J. B. (1993). The lift on a small sphere in wall-bounded linear shear flows. *J. Fluid Mech.*, *246*: 249-265.

998 [90] Krishnan, G. P. & Leighton Jr, D. T. (1995). Inertial lift on a moving sphere in contact with
999 a plane wall in a shear flow. *Phys. Fluids, 7*: 2538-2545.

1000 [91] Patankar, N. A., Huang, P. Y., Ko, T., Joseph, D. D. (2001). Lift-off of a single particle in
1001 Newtonian and viscoelastic fluids by direct numerical simulation. *J. Fluid Mech., 438*: 67-100.

1002 [92] Takemura, F., Takagi, S., Magnaudet, J., Matsumoto, Y. (2002). Drag and lift forces on a
1003 bubble rising near a vertical wall in a viscous liquid. *J. Fluid Mech., 461*: 277-300.

1004 [93] Zeng, L., Balachandar, S., Fischer, P. (2005). Wall-induced forces on a rigid sphere at finite
1005 Reynolds number. *J. Fluid Mech., 536*: 1-25.

1006 [94] Tippayawong, N. & Preechawuttipong, I. (2011). Analytical prediction of particle
1007 detachment from a flat surface by turbulent air flows. *Chiang Mai J. Sci.* 38: 503-507.

1008